ACSNANO

www.acsnano.org

ARTICLE

Directing Organometallic Ring−Chain Equilibrium by Electrostatic Interactions

Rujia Hou, Yuhong Gao, Yuan Guo, Chi Zhang,* and Wei Xu*

Cite This: *ACS Nano* 2024, 18, 31478−31484

Read Online

ACCESS | Metrics & More | Article Recommendations | Supporting Information

ABSTRACT: **Dynamic chemistry, which falls into the realm of both supramolecular and covalent chemistry, enables intriguing properties, such as structural diversity, self-healing, and adaptability. Due to robustness of covalent bonds compared to noncovalent ones, dynamic covalent chemistry has been exploited to synthesize complex molecular nanostructures at solid/liquid interfaces under ambient conditions, generally responsive to internal factors that directly regulate intermolecular covalent bonds. However, directing dynamics of covalent nanostructures, *e.g.*, the typical ring−chain equilibria, on surface by extrinsic interactions remains elusive and challenging. Herein, we have controllably directed the ring−chain equilibrium of covalent organometallic structures by regulating intermolecular electrostatic interactions, thus achieving on-surface dynamic covalent chemistry under ultrahigh vacuum conditions. Our findings unravel the dynamic mechanism of covalent polymers governed by weak intermolecular interactions at the submolecular level, which not only bridges the gap between supramolecular and covalent chemistry but also offers great opportunities for the fabrication of adaptive polymeric nanostructures that respond to different conditions.**

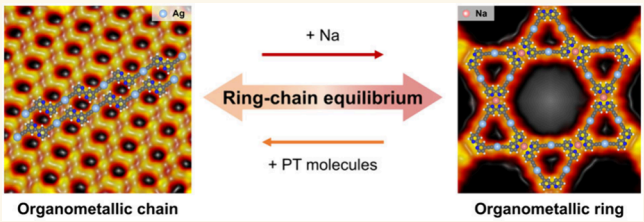

KEYWORDS: *on-surface chemistry, dynamic covalent chemistry, ring−chain equilibrium, scanning tunneling microscopy, density functional theory*

Dynamic chemistry,[1] by virtue of reversible formation and cleavage of bonds (either covalent or noncovalent) in response to internal factors or external stimuli, enables molecular and supramolecular diversity and gives access to functional architectures with intriguing properties such as self-healing and adaptability.[2−4] Among others, noncovalent interactions take advantage of their labile nature to access structural diversity through various regulatory factors,[5−7] resulting in relatively fragile architectures with limited stability. Notably, dynamic covalent chemistry,[8−10] typically like the ring−chain equilibria,[10−12] based on reversible covalent bonds among molecular building blocks, allows structural fracture and reorganization to induce macroscopic morpho-logical material transformations[11,12] and provides opportunities for adaptive dynamic polymers[13] featured with both the adaptability of supramolecular chemistry and the robustness of covalent bonding. In this regard, on-surface chemistry serves as a promising platform to resolve and steer a wide range of intermolecular interactions,[6,14,15] ranging from noncovalent[16] to covalent,[17] and to unravel the synergism and competition mechanisms of these interactions, leading to the controllable regulation and construction of nanostructures. Tremendous effort has been devoted to exploring dynamic covalent chemistry at solid/liquid interfaces under ambient conditions, generally in the presence of water,[18−23] such as Schiff-base reactions,[18,19] dynamic exchanges of bisimines,[20] condensation of boronic acids,[22] and Knoevenagel polycondensation.[23] Such processes are mainly responsive to internal factors, such as molecular components, time, concentration, and temperature. However, whether extrinsic intermolecular interactions provide access to the dynamics of covalent nanostructures remains elusive and challenging. Therefore, it is of utmost interest to explore the possibility of steering the dynamics of covalent polymers by fine-tuning intermolecular interactions and to visualize their evolution at the submolecular level, which should be significant for the fundamental understanding of dynamic covalent chemistry.

In this study, the ring−chain equilibrium of covalent organometallic structures was directed on Ag(111) at room temperature by subtly regulating intermolecular electrostatic interactions (Scheme 1). The molecular precursor, 4,4′-diethynyl-2,2′-bipyridine (abbreviated as DEBPy), was se-

Received: August 30, 2024
Revised: October 18, 2024
Accepted: October 23, 2024
Published: October 30, 2024

https://doi.org/10.1021/acsnano.4c12046
ACS Nano 2024, 18, 31478−31484

Scheme 1. Ring−Chain Equilibrium between the DEBPy-Based Covalent Organometallic Chains and Rings[a]

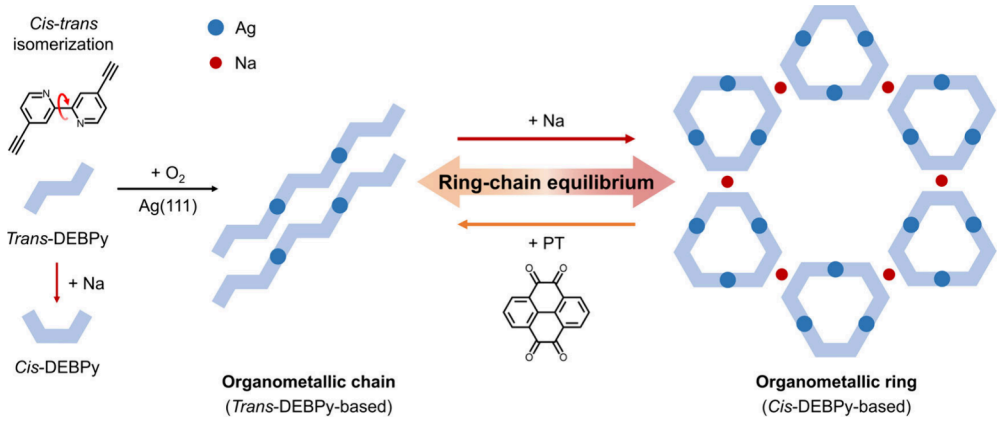

[a]Left panel: Na-induced *trans*-to-*cis* isomerization of DEBPy by flipping around the C−C bond. *Trans*- and *cis*-forms are indicated by the blue Z-shaped and C-shaped silhouettes, respectively. Ag: dark blue dots; Na: red dots.

lected, consisting of two terminal alkynyl groups (for the construction of C_{sp}−Ag−C_{sp} organometallic bonds[24]) and a bipyridyl moiety (as the potential site for interacting with extrinsic metal atoms[15,25,26]). Organometallic (OM) bonding (*i.e.*, C−M−C) combines both covalent[27] and reversible[28] properties and has the potential to be tailored to produce distinct covalent OM polymers, thereby qualifying it as a member of the dynamic covalent bond family. Specifically, metal−C_{sp} bonds are generally more robust than metal−C_{aryl} bonds due to their increased *s*-character, providing an interesting model system to be further steered by intermolecular interactions. Despite their significance, the dynamics of C−M−C covalent bonds has not been systematically explored. Based on scanning tunneling microscopy (STM) imaging and density functional theory (DFT) calculations, *trans*-DEBPy-based organometallic chains (*trans* OM chains) were first constructed after dosing O_2[24] onto the DEBPy-precovered Ag(111) surface. By further introduction of Na atoms, on the basis of dynamic C_{sp}−Ag−C_{sp} OM bonding, *trans* OM chains were converted to *cis*-DEBPy-based organometallic rings (*cis* OM rings), resulting from electrostatic interactions between Na and bipyridyl moieties. More interestingly, by introduction of pyrene-4,5,9,10-tetraone (abbreviated as PT) molecules, the *cis* OM rings were converted back to the *trans* OM chains via the removal of Na (due to stronger interactions between Na and diketone moieties of PT). Therefore, by regulation of the intermolecular electrostatic interactions, the covalent OM ring−chain interconversion has been successfully achieved on Ag(111) at room temperature, where the *cis-trans* isomerization determined by such intermolecular interactions was revealed to be the key to the dynamic covalent evolution.

RESULTS AND DISCUSSION

After deposition of DEBPy molecules onto Ag(111) at room temperature (RT, ∼300 K), a well-ordered self-assembled structure was formed (Figure 1a), where all the molecules are in the *trans*-form[29] with a Z-shaped morphology, as referred to the silhouette and the superimposed molecular model (Figure 1b). The DFT-optimized single *trans*-DEBPy molecule adsorbed on Ag(111) is shown in Figure 1c with a flat-lying configuration. The STM simulation (the gray part in Figure 1b) is also superimposed on the STM image in good agreement. Subsequently, the alkali metal Na was introduced

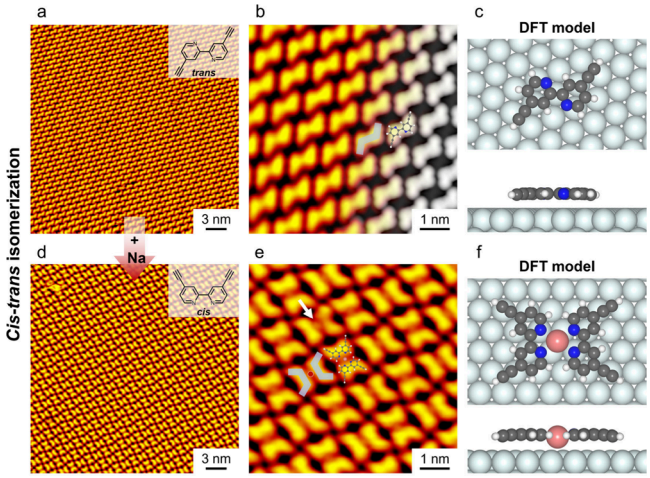

Figure 1. Na-induced *trans*-to-*cis* isomerization of DEBPy molecules on Ag(111). (a) Large-scale and (b) close-up STM images showing the self-assembled structure of *trans*-DEBPy on Ag(111). (c) Top and side views of the DFT-optimized *trans*-DEBPy molecule adsorbed on Ag(111). (d) Large-scale and (e) close-up STM images showing the formation of metal−organic dimers composed of *cis*-DEBPy and Na. (f) Top and side views of the DFT-optimized metal−organic dimer structure. Scanning conditions: $V = -1.2$ V, $I = 0.6$ nA. C: gray; H: white; N: navy blue; Na: pink; Ag substrate: light blue.

to provide extrinsic intermolecular electrostatic interactions[25,30,31] with the bipyridyl moieties. After dosing Na atoms onto the *trans*-DEBPy-precovered Ag(111) sample (Figure 1a) held at RT, it was found that DEBPy molecules were all dimerized as shown in Figure 1d, and each Z-shaped *trans*-DEBPy molecule was converted to a C-shaped *cis*-form as identified from the magnified STM image (Figure 1e), where an individual dimer is indicated by the superimposed silhouette. In a special tip state, a central dim spot was visible (indicated by the white arrow) and attributed to a single Na[32,33] (Figure 1e). Accordingly, the DFT-calculated metal−organic dimer structure (Figure 1f) is superimposed in Figure 1e, where two *cis*-DEBPy molecules interact with the central Na via 4-fold Na···N electrostatic interactions.[26] Thus, by introduction of Na atoms, the resulting intermolecular electrostatic interactions successfully induced the *trans*-to-*cis*

https://doi.org/10.1021/acsnano.4c12046
ACS Nano 2024, 18, 31478−31484

isomerization and the formation of dimer structures with high efficiency.

To explore the dynamics of covalent OM structures driven by extrinsic intermolecular interactions, covalent OM chain structure (Figure 2a) was first constructed by exposing the

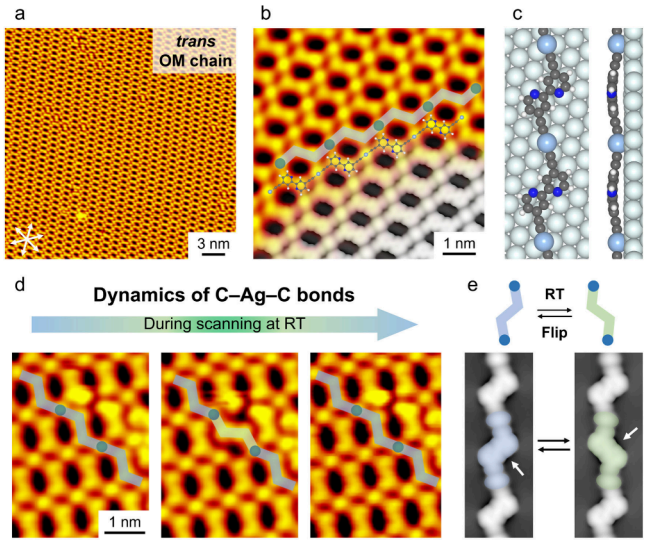

Figure 2. Construction of *trans* OM chains from DEBPy on Ag(111) and observation of the dynamics of C−Ag−C bonds involved. (a) Large-scale and (b) close-up STM images showing the formation of *trans* OM chains, superimposed with the silhouette for a single chain, corresponding DFT-optimized model, and STM simulation (the gray part). (c) DFT-optimized *trans* OM chain on Ag(111). C: gray; H: white; N: navy blue; Ag substrate: light blue; Ag adatom: sky-blue. (d) Sequential STM images recorded in the same region showing reversible molecular flips (indicated by light blue and green Z-shaped silhouettes, respectively) in the *trans* OM chains during scanning at RT. (e) STM simulations of a single OM chain with reversible molecular flips. Scanning conditions: $V = -1.2$ V, $I = 0.6$ nA. The close-packed directions of Ag(111) are indicated by white arrows in (a).

trans-DEBPy-precovered surface held at RT (refer to Figure 1a) to O_2 for 20 min at a pressure of ∼1 × 10^{-7} mbar, following the reported strategy.[24] Based on the previous reports,[24,34] the C−H activation of terminal alkynes on Ag(111) can be triggered by introducing O_2 at RT, leading to the formation of C_{sp}−Ag−C_{sp} bonded OM structures. From the magnified STM image (Figure 2b), it is seen that the OM chain structure is composed of dehydrogenated *trans*-DEBPy molecules and Ag adatoms. The DFT-optimized single OM chain on Ag(111) is shown in Figure 2c, which is also superimposed on the STM image together with the STM simulation (the gray part in Figure 2b).

Intriguingly, during the scanning of the OM chains at RT, continuous flips of molecular components (*i.e.*, the dehydrogenated *trans*-DEBPy) were also observed, as shown in Figure 2d and further detailed in Figure S1, indicating the cleavage and reformation of C_{sp}−Ag−C_{sp} bonds[35] in the *trans* OM chains at RT.[28] To exclude the perturbation from scanning, such a sample was also scanned at ∼100 K using the same scanning parameters, and the target regions remained unchanged, thereby verifying the dynamics of C_{sp}−Ag−C_{sp} bonds at RT (Figure S2). Notably, molecular flips can also occur at much lower bias voltages (*e.g.*, − 0.3 V) at RT, further excluding the influence of scanning. In addition, STM simulations (Figure 2e) were performed on a single OM chain to mimic such a situation, consistent with the corresponding experimental morphologies displayed in Figure 2d. The reaction pathways for the cleavage and reformation of the C_{sp}−Ag−C_{sp} bond on Ag(111) were also calculated based on an OM dimer for simplicity, with energy barriers of ∼0.97 eV and ∼0.22 eV for the cleavage and reformation, respectively (Figure S3).

As shown above, Na-induced *trans*-to-*cis* isomerization of single DEBPy molecules was achieved with a high efficiency. Inspired by this together with the dynamic characteristics of C_{sp}−Ag−C_{sp} bonds, an interesting question arises whether extrinsic Na could induce more complicated structural conversions of covalent OM polymers by regulating intermolecular electrostatic interactions? To explore this, a series of experiments were performed by gradually introducing Na atoms and tracking the resulting submolecular evolution in real space (see Figure S4 for more details). Surprisingly, after the addition of Na atoms to the *trans* OM chains (Figure 3a) at RT, the dynamic evolution from *trans* OM chains to Kagome networks composed of *cis* OM rings was observed (Figure 3b). A closer inspection (Figure 3c) reveals that each *cis* OM ring is composed of three *cis*-DEBPy-based components and three Ag adatoms, and such OM rings are linked together via Na (as indicated by the silhouettes), similar to the case of single *cis*-DEBPy molecules (refer to Figure 1e). The DFT-optimized structural model combined with the corresponding STM simulation is shown in Figure 3d. A close-up STM image of such a Kagome network superimposed with the molecular model is shown in Figure 3e. Note that due to the expanded pore size in *cis* OM rings compared to *trans* OM chains, the chain-to-ring conversion also depends on the initial coverage of molecular precursors, which is consistent with previous reports.[36,37] Consequently, the formation of such extended Kagome networks requires sufficient surface space, with a preference for lower molecular coverage.

More interestingly, by introduction of PT molecules to "remove" Na from the Kagome network at RT, the *cis* OM rings were converted back to the *trans* OM chains (Figure 3f). Such a scenario is rationalized by the DFT calculations (detailed in Figure S5), which indicate that the interactions between Na and diketone moieties of PT are stronger than those between Na and bipyridyl moieties of *cis*-DEBPy. The coexistence of separated *trans* OM chains and PT+Na structure, colored green and brown, respectively, is shown in Figure 3f and g. The DFT-optimized structural model of PT +Na shows that the adjacent PT molecules are aligned in a row via 4-fold Na···O electrostatic interactions, similar to the situations with the integration of other metal atoms,[38,39] and then extend to form close-packed islands (Figure 3h). The corresponding STM simulation (the gray part) also reproduces the experimental morphology. In addition, a control experiment involving the deposition of PT molecules and Na atoms on Ag(111) confirmed the characteristic PT+Na structure (as observed in Figure S6). Moreover, the driving force for this dynamic evolution process is revealed by DFT calculations on the total energies of molecular systems with the same molecular components, involving different binding sites of Na and different molecular conformations of DEBPy (Figure 3i and more details in Figure S7). It is energetically more favorable for Na to interact with *cis*-DEBPy molecules (via 4-fold Na···N electrostatic interactions) than with *trans*-ones (via 2-fold Na···N interactions), consistent with the chain-to-ring

https://doi.org/10.1021/acsnano.4c12046
ACS Nano 2024, 18, 31478−31484

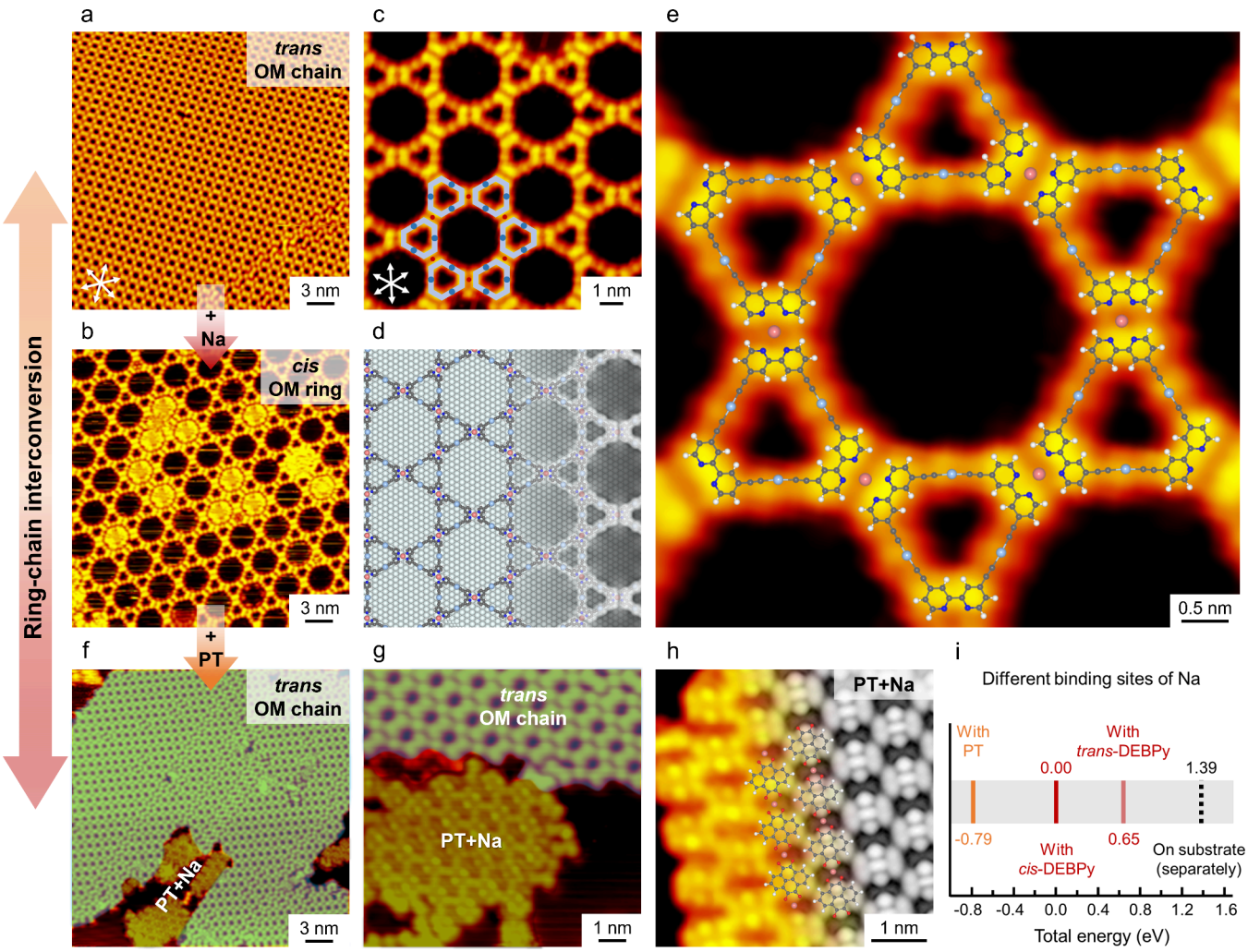

Figure 3. Ring−chain interconversion between *trans* OM chains and *cis* OM rings on Ag(111) at RT. (a, b) Large-scale STM images showing the Na-induced chain-to-ring conversion from (a) *trans* OM chains to (b) *cis* OM rings. (c) Magnified STM image of *cis* OM rings superimposed with the corresponding silhouettes. (d) DFT-optimized structural model (left) and corresponding STM simulation (right). (e) Submolecularly resolved STM image of *cis* OM rings overlaid with the DFT-optimized model. (f) Large-scale STM image showing the PT-induced ring-to-chain conversion at RT, with the coexistence of PT+Na islands. (g) Zoomed-in STM image showing the coexistence of *trans* OM chains and PT+Na islands colored in green and brown, respectively. (h) High-resolution STM image of the PT+Na structure overlaid with the corresponding DFT-optimized model and STM simulation (the gray part). Scanning conditions: $V = -1.2$ V, $I = 0.6$ nA. (i) Total energies of molecular systems involving two DEBPy molecules, two PT molecules, and one Na atom coadsorbed on Ag(111) with different binding sites of Na and different molecular conformations of DEBPy, given with respect to that of the "with *cis*-DEBPy" structure (set to zero for reference). C: gray; H: white; N: navy blue; Na: pink; O: red; Ag substrate: light blue; Ag adatom: sky-blue.

conversion. Additionally, Na prefers to interact with PT molecules (via 4-fold Na···O interactions) rather than with *cis*-DEBPy molecules, in line with the ring-to-chain conversion via the removal of Na. Therefore, by regulation of the intermolecular electrostatic interactions, OM ring−chain interconversion has been successfully achieved on Ag(111). It is particularly noteworthy that the entire interconversion process occurs at constant RT, suggesting that the entropy change is almost negligible.

To further unravel the mechanism for the dynamic evolution processes and to reveal the role of Na, DFT calculations were performed, as displayed in Figure 4. As shown in the upper panel, for a single DEBPy molecule, the *trans*-conformation (IS) is energetically more stable than the *cis*-one (FS) on Ag(111), by 0.28 eV, consistent with the experimental observation. Such a *trans*-to-*cis* isomerization has an energy barrier of ∼0.68 eV and is endothermic, indicating that the *trans*-to-*cis* isomerization is thermodynamically unfavorable.

By contrast, by adding a Na atom to the molecular system with two *trans*-DEBPy molecules (as shown in the lower panel), the Na atom initially interacts with two opposite N sites of the *trans*-molecules via 2-fold Na···N electrostatic interactions, forming the Na-interlinked *trans*-dimer (IS_Na, which is captured experimentally as shown in Figure S4), which is energetically more favorable than the situation without any interactions (IS+Na), by 0.75 eV. Subsequently, with the assistance of the Na atom, the *trans*-dimer underwent a two-step *trans*-to-*cis* isomerization, with energy barriers of ∼0.38 eV and ∼0.40 eV, respectively, forming the energetically more stable metal−organic *cis*-dimer via 4-fold Na···N electrostatic interactions. Thus, in the presence of Na, the *trans*-to-*cis* isomerization is converted from endothermic to exothermic, which explains the chain-to-ring conversion at RT.

https://doi.org/10.1021/acsnano.4c12046
ACS Nano 2024, 18, 31478−31484

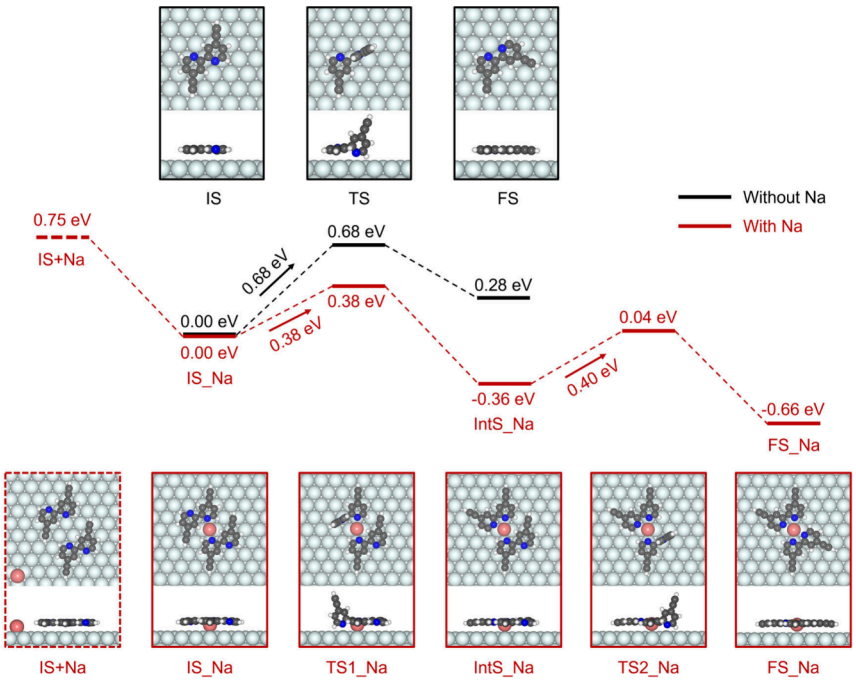

Figure 4. DFT-calculated reaction pathways for the *cis-trans* interconversion of a DEBPy molecule and a Na-interlinked dimer on Ag(111) without and with the assistance of Na (upper and lower panels), respectively. The structural models of the initial states (IS, IS_Na), transition states (TS, TS_Na), intermediate state (IntS_Na) and final states (FS, FS_Na) are presented, and their energies are provided with respect to those of the corresponding IS. C: gray; H: white; N: navy blue; Na: pink; Ag substrate: light blue.

Notably, after the addition of PT molecules, the competitive preference of PT to interact with Na over *cis*-DEBPy (cf. Figure 3i) results in the removal of Na and allows the reverse *cis*-to-*trans* isomerization accompanied by the ring-to-chain conversion.

CONCLUSIONS

In conclusion, by combining STM imaging and DFT calculations, we have controllably directed the organometallic ring−chain equilibrium on Ag(111) at RT by subtly regulating weak intermolecular interactions. *Cis-trans* isomerization in response to Na, together with the dynamics of C−Ag−C bonds, was identified as the key to such processes and rationalized by theoretical calculations. The dynamic evolution processes of ring−chain interconversion were also visualized at the submolecular level. Our findings unravel the dynamics of covalent organometallic polymers governed by relatively weak intermolecular electrostatic interactions, which should integrate both the adaptability of supramolecular chemistry and the robustness of covalent bonding, and offer great opportunities for the fabrication of adaptive polymeric nanostructures.

METHODS

STM Measurements. All the STM experiments were performed in an ultrahigh vacuum chamber with a base pressure of ∼1.0×10^{-10} mbar, which was equipped with a variable-temperature, fast-scanning "Aarhus-type" STM using electrochemically etched tungsten (W) tips.[40,41] The Ag(111) substrate was cleaned by Ar^+-ion sputtering and annealing at ∼800 K for repeated cycles. After thorough degassing, the DEBPy and PT molecules (purchased from Bidepham, with purities of >98%) were sublimated separately by two homemade Knudsen-cells at ∼330 and ∼450 K, respectively. The alkali metal Na (from SAES Getters) was dosed via conventional resistance heating after fully degassing. Oxygen molecules were dosed through a leak valve onto the DEBPy-precovered Ag(111) sample, which was held at RT in the preparation chamber at a pressure of ∼1×10^{-7} mbar for 20 min. The STM images were typically recorded at 100−150 K (unless otherwise noted) and further smoothed to eliminate noises.

Theoretical Calculations. The calculations were performed in the framework of DFT by using the Vienna ab initio simulation package (VASP).[42,43] The projector-augmented wave method was used to describe the interaction between ions and electrons.[44,45] The Perdew−Burke−Ernzerhof generalized gradient approximation exchange-correlation functional was employed,[46] and van der Waals interactions were included using the dispersion-corrected DFT-D3 method of Grimme.[47] The atomic structures were relaxed using the conjugate gradient algorithm scheme as implemented in the VASP code until the forces on all unconstrained atoms were ≤0.03 eV/Å. Plane waves were used as a basis set with an energy cutoff of 400 eV. For the structural models, the Ag(111) substrates were modeled by three-layered slabs separated by a ∼15 Å vacuum region, where the bottom layer was fixed. Reaction pathways were calculated by a combination of the climbing image-nudged elastic band (CI-NEB)[48] and dimer methods[49] until the forces acting on the path typically converged to ≤0.03 eV/Å.

ASSOCIATED CONTENT

Supporting Information

The Supporting Information is available free of charge at https://pubs.acs.org/doi/10.1021/acsnano.4c12046.

Supplementary STM images and DFT calculations (PDF)

AUTHOR INFORMATION

Corresponding Authors

Chi Zhang − *Interdisciplinary Materials Research Center, School of Materials Science and Engineering, Tongji University, Shanghai 201804, People's Republic of China;* orcid.org/0000-0002-2335-4579; Email: zhangchi11@tongji.edu.cn

https://doi.org/10.1021/acsnano.4c12046
ACS Nano 2024, 18, 31478−31484

Wei Xu − *Interdisciplinary Materials Research Center, School of Materials Science and Engineering, Tongji University, Shanghai 201804, People's Republic of China*; orcid.org/0000-0003-0216-794X; Email: xuwei@tongji.edu.cn

Authors

Rujia Hou − *Interdisciplinary Materials Research Center, School of Materials Science and Engineering, Tongji University, Shanghai 201804, People's Republic of China*

Yuhong Gao − *Interdisciplinary Materials Research Center, School of Materials Science and Engineering, Tongji University, Shanghai 201804, People's Republic of China*

Yuan Guo − *Interdisciplinary Materials Research Center, School of Materials Science and Engineering, Tongji University, Shanghai 201804, People's Republic of China*

Complete contact information is available at: https://pubs.acs.org/10.1021/acsnano.4c12046

Author Contributions

The manuscript was written through contributions of all authors. All authors have given approval to the final version of the manuscript.

Notes

The authors declare no competing financial interest.

ACKNOWLEDGMENTS

The authors acknowledge financial support from the National Natural Science Foundation of China (grants nos. 22202153 and 22125203) and the Fundamental Research Funds for the Central Universities. This work also used computational resources of the Supercomputer HOKUSAI BigWaterfull 2 provided by RIKEN through the HPCI System Research Project (project ID: hp240096).

REFERENCES

(1) Lehn, J.-M. From Supramolecular Chemistry towards Constitutional Dynamic Chemistry and Adaptive Chemistry. *Chem. Soc. Rev.* **2007**, *36*, 151−160.

(2) Wang, S.; Urban, M. W. Self-Healing Polymers. *Nat. Rev. Mater.* **2020**, *5*, 562−583.

(3) Li, B.; Cao, P.-F.; Saito, T.; Sokolov, A. P. Intrinsically Self-Healing Polymers: From Mechanistic Insight to Current Challenges. *Chem. Rev.* **2023**, *123*, 701−735.

(4) Fuhrmann, A.; Göstl, R.; Wendt, R.; Kötteritzsch, J.; Hager, M. D.; Schubert, U. S.; Brademann-Jock, K.; Thünemann, A. F.; Nöchel, U.; Behl, M.; Hecht, S. Conditional Repair by Locally Switching the Thermal Healing Capability of Dynamic Covalent Polymers with Light. *Nat. Commun.* **2016**, *7*, 13623.

(5) Kühne, D.; Klappenberger, F.; Krenner, W.; Klyatskaya, S.; Ruben, M.; Barth, J. V. Rotational and Constitutional Dynamics of Caged Supramolecules. *Proc. Natl. Acad. Sci. U. S. A.* **2010**, *107*, 21332−21336.

(6) Kong, H.; Zhang, C.; Xie, L.; Wang, L.; Xu, W. Constitutional Dynamics of Metal−Organic Motifs on a Au(111) Surface. *Angew. Chem., Int. Ed.* **2016**, *55*, 7157−7160.

(7) Zhang, C.; Wang, L.; Xie, L.; Ding, Y.; Xu, W. On-Surface Dual-Response Structural Transformations of Guanine Molecules and Fe Atoms. *Chem. Eur. J.* **2017**, *23*, 2356−2362.

(8) Zhang, W.; Chen, L.; Dai, S.; Zhao, C.; Ma, C.; Wei, L.; Zhu, M.; Chong, S. Y.; Yang, H.; Liu, L.; Bai, Y.; Yu, M.; Xu, Y.; Zhu, X.-W.; Zhu, Q.; An, S.; Sprick, R. S.; Little, M. A.; Wu, X.; Jiang, S.; et al. Reconstructed Covalent Organic Frameworks. *Nature* **2022**, *604*, 72−79.

(9) Liu, H.; Lu, H.-H.; Zhuang, J.; Thayumanavan, S. Three-Component Dynamic Covalent Chemistry: From Janus Small Molecules to Functional Polymers. *J. Am. Chem. Soc.* **2021**, *143*, 20735−20746.

(10) Rowan, S. J.; Cantrill, S. J.; Cousins, G. R. L.; Sanders, J. K. M.; Stoddart, J. F. Dynamic Covalent Chemistry. *Angew. Chem., Int. Ed.* **2002**, *41*, 898−952.

(11) Maeda, T.; Otsuka, H.; Takahara, A. Dynamic Covalent Polymers: Reorganizable Polymers with Dynamic Covalent Bonds. *Prog. Polym. Sci.* **2009**, *34*, 581−604.

(12) Wojtecki, R. J.; Meador, M. A.; Rowan, S. J. Using the Dynamic Bond to Access Macroscopically Responsive Structurally Dynamic Polymers. *Nat. Mater.* **2011**, *10*, 14−27.

(13) Roy, N.; Bruchmann, B.; Lehn, J.-M. DYNAMERS: Dynamic Polymers as Self-Healing Materials. *Chem. Soc. Rev.* **2015**, *44*, 3786−3807.

(14) Xie, L.; Ding, Y.; Li, D.; Zhang, C.; Wu, Y.; Sun, L.; Liu, M.; Qiu, X.; Xu, W. Local Chiral Inversion of Thymine Dimers by Manipulating Single Water Molecules. *J. Am. Chem. Soc.* **2022**, *144*, 5023−5028.

(15) Yi, Z.; Guo, Y.; Hou, R.; Zhang, Z.; Gao, Y.; Zhang, C.; Xu, W. Revealing the Orientation Selectivity of Tetrapyridyl-Substituted Porphyrins Constrained in Molecular "Klotski Puzzles. *J. Am. Chem. Soc.* **2023**, *145*, 22366−22373.

(16) Zhang, C.; Xu, W. Interactions between Water and Organic Molecules or Inorganic Salts on Surfaces. *Aggregate* **2022**, *3*, No. e175.

(17) Zhang, C.; Yi, Z.; Xu, W. Scanning Probe Microscopy in Probing Low-Dimensional Carbon-Based Nanostructures and Nanomaterials. *Mater. Futures* **2022**, *1*, No. 032301.

(18) Liu, X.-H.; Guan, C.-Z.; Ding, S.-Y.; Wang, W.; Yan, H.-J.; Wang, D.; Wan, L.-J. On-Surface Synthesis of Single-Layered Two-Dimensional Covalent Organic Frameworks *via* Solid-Vapor Interface Reactions. *J. Am. Chem. Soc.* **2013**, *135*, 10470−10474.

(19) Xu, L.; Zhou, X.; Yu, Y.; Tian, W. Q.; Ma, J.; Lei, S. Surface-Confined Crystalline Two-Dimensional Covalent Organic Frameworks *via* On-Surface Schiff-Base Coupling. *ACS Nano* **2013**, *7*, 8066−8073.

(20) Ciesielski, A.; El Garah, M.; Haar, S.; Kovaříček, P.; Lehn, J.-M.; Samorì, P. Dynamic Covalent Chemistry of Bisimines at the Solid/Liquid Interface Monitored by Scanning Tunnelling Microscopy. *Nat. Chem.* **2014**, *6*, 1017−1023.

(21) Liu, C.; Park, E.; Jin, Y.; Liu, J.; Yu, Y.; Zhang, W.; Lei, S.; Hu, W. Surface-Confined Dynamic Covalent System Driven by Olefin Metathesis. *Angew. Chem., Int. Ed.* **2018**, *57*, 1869−1873.

(22) Zhan, G.; Cai, Z.-F.; Strutyński, K.; Yu, L.; Herrmann, N.; Martínez-Abadía, M.; Melle-Franco, M.; Mateo-Alonso, A.; Feyter, De S. Observing Polymerization in 2D Dynamic Covalent Polymers. *Nature* **2022**, *603*, 835−840.

(23) Fabozzi, F. G.; Severin, N.; Rabe, J. P.; Hecht, S. Room Temperature On-Surface Synthesis of a Vinylene-Linked Single Layer Covalent Organic Framework. *J. Am. Chem. Soc.* **2023**, *145*, 18205−18209.

(24) Zhang, C.; Kazuma, E.; Kim, Y. Steering the Reaction Pathways of Terminal Alkynes by Introducing Oxygen Species: From C−C Coupling to C−H Activation. *J. Am. Chem. Soc.* **2022**, *144*, 10282−10290.

(25) Liu, X.; Matej, A.; Kratky, T.; Mendieta-Moreno, J. I.; Günther, S.; Mutombo, P.; Decurtins, S.; Aschauer, U.; Repp, J.; Jelinek, P.; Liu, S.-X.; Patera, L. L. Exploiting Cooperative Catalysis for the On-Surface Synthesis of Linear Heteroaromatic Polymers *via* Selective C−H Activation. *Angew. Chem., Int. Ed.* **2022**, *61*, No. e202112798.

(26) Hou, R.; Guo, Y.; Yi, Z.; Zhang, Z.; Zhang, C.; Xu, W. Construction and Structural Transformation of Metal−Organic Nanostructures Induced by Alkali Metals and Alkali Metal Salts. *J. Phys. Chem. Lett.* **2023**, *14*, 3636−3642.

(27) Li, S.; Yu, H.; Chen, X.; Gewirth, A. A.; Moore, J. S.; Schroeder, C. M. Covalent Ag−C Bonding Contacts from Unprotected Terminal Acetylenes for Molecular Junctions. *Nano Lett.* **2020**, *20*, 5490−5495.

(28) Fan, Q.; Wang, C.; Han, Y.; Zhu, J.; Kuttner, J.; Hilt, G.; Gottfried, J. M. Surface-Assisted Formation, Assembly, and Dynamics

of Planar Organometallic Macrocycles and Zigzag Shaped Polymer Chains with C−Cu−C Bonds. *ACS Nano* **2014**, *8*, 709−718.
(29) Li, X.; Niu, K.; Duan, S.; Tang, Y.; Hao, Z.; Xu, Z.; Ge, H.; Rosen, J.; Björk, J.; Zhang, H.; Xu, X.; Chi, L. Pyridinic Nitrogen Modification for Selective Acetylenic Homocoupling on Au(111). *J. Am. Chem. Soc.* **2023**, *145*, 4545−4552.
(30) Shan, H.; Zhou, L.; Ji, W.; Zhao, A. Flexible Alkali−Halogen Bonding in Two Dimensional Alkali-Metal Organic Frameworks. *J. Phys. Chem. Lett.* **2021**, *12*, 10808−10814.
(31) Zhang, Z.; Gao, Y.; Yi, Z.; Zhang, C.; Xu, W. Separation of Halogen Atoms by Sodium from Dehalogenative Reactions on a Au(111) Surface. *ACS Nano* **2024**, *18*, 9082−9091.
(32) Zhang, C.; Wang, L.; Xie, L.; Kong, H.; Tan, Q.; Cai, L.; Sun, Q.; Xu, W. Solventless Formation of G-Quartet Complexes Based on Alkali and Alkaline Earth Salts on Au(111). *ChemPhysChem* **2015**, *16*, 2099−2105.
(33) Ding, Y.; Wang, X.; Li, D.; Xu, W. Real-Space Evidence of Trimeric, Tetrameric, and Pentameric Uracil Clusters Induced by Alkali Metals. *J. Phys. Chem. C* **2020**, *124*, 5257−5262.
(34) Zhang, Y.-Q.; Paintner, T.; Hellwig, R.; Haag, F.; Allegretti, F.; Feulner, P.; Klyatskaya, S.; Ruben, M.; Seitsonen, A. P.; Barth, J. V.; Klappenberger, F. Synthesizing Highly Regular Single-Layer Alkynyl−Silver Networks at the Micrometer Scale *via* Gas-Mediated Surface Reaction. *J. Am. Chem. Soc.* **2019**, *141*, 5087−5091.
(35) Fan, Q.; Wang, T.; Dai, J.; Kuttner, J.; Hilt, G.; Gottfried, J. M.; Zhu, J. On-Surface Pseudo-High-Dilution Synthesis of Macrocycles: Principle and Mechanism. *ACS Nano* **2017**, *11*, 5070−5079.
(36) Walch, H.; Dienstmaier, J.; Eder, G.; Gutzler, R.; Schlögl, S.; Sirtl, T.; Das, K.; Schmittel, M.; Lackinger, M. Extended Two-Dimensional Metal−Organic Frameworks Based on Thiolate−Copper Coordination Bonds. *J. Am. Chem. Soc.* **2011**, *133*, 7909−7915.
(37) Mo, Y.-P.; Liu, X.-H.; Wang, D. Concentration-Directed Polymorphic Surface Covalent Organic Frameworks: Rhombus, Parallelogram, and Kagome. *ACS Nano* **2017**, *11*, 11694−11700.
(38) Song, X.; Zhou, Z.; Peng, X.; Liu, X.; Han, D.; Zhang, H.; Liu, X.; Wang, L.; Kong, H. Structural Phase Transition of Quinone-Containing PAH Derivatives on Au(111) at High Coverage. *J. Phys. Chem. C* **2023**, *127*, 5039−5043.
(39) Della Pia, A.; Riello, M.; Lawrence, J.; Stassen, D.; Jones, T. S.; Bonifazi, D.; De Vita, A.; Costantini, G. Two-Dimensional Ketone-Driven Metal−Organic Coordination on Cu(111). *Chem. Eur. J.* **2016**, *22*, 8105−8112.
(40) Besenbacher, F. Scanning Tunnelling Microscopy Studies of Metal Surfaces. *Rep. Prog. Phys.* **1996**, *59*, 1737−1802.
(41) Laegsgaard, E.; Österlund, L.; Thostrup, P.; Rasmussen, P. B.; Stensgaard, I.; Besenbacher, F. A High-Pressure Scanning Tunneling Microscope. *Rev. Sci. Instrum.* **2001**, *72*, 3537−3542.
(42) Kresse, G.; Hafner, J. Ab Initio Molecular Dynamics for Open-Shell Transition Metals. *Phys. Rev. B* **1993**, *48*, 13115−13118.
(43) Kresse, G.; Furthmüller, J. Efficient Iterative Schemes for Ab Initio Total-Energy Calculations Using a Plane-Wave Basis Set. *Phys. Rev. B* **1996**, *54*, 11169−11186.
(44) Blöchl, P. E. Projector Augmented-Wave Method. *Phys. Rev. B* **1994**, *50*, 17953−17979.
(45) Kresse, G.; Joubert, D. From Ultrasoft Pseudopotentials to the Projector Augmented-Wave Method. *Phys. Rev. B* **1999**, *59*, 1758−1775.
(46) Perdew, J. P.; Burke, K.; Ernzerhof, M. Generalized Gradient Approximation Made Simple. *Phys. Rev. Lett.* **1996**, *77*, 3865−3868.
(47) Grimme, S.; Antony, J.; Ehrlich, S.; Krieg, H. A Consistent and Accurate Ab Initio Parametrization of Density Functional Dispersion Correction (DFT-D) for the 94 Elements H-Pu. *J. Chem. Phys.* **2010**, *132*, No. 154104.
(48) Henkelman, G.; Uberuaga, B. P.; Jónsson, H. A Climbing Image Nudged Elastic Band Method for Finding Saddle Points and Minimum Energy Paths. *J. Chem. Phys.* **2000**, *113*, 9901−9904.
(49) Kästner, J.; Sherwood, P. Superlinearly Converging Dimer Method for Transition State Search. *J. Chem. Phys.* **2008**, *128*, No. 014106.

https://doi.org/10.1021/acsnano.4c12046
ACS Nano 2024, 18, 31478−31484